Volume 8
Number 43
21 November 2020
Pages 14963–15472

Journal of Materials Chemistry C

Materials for optical, magnetic and electronic devices

rsc.li/materials-c

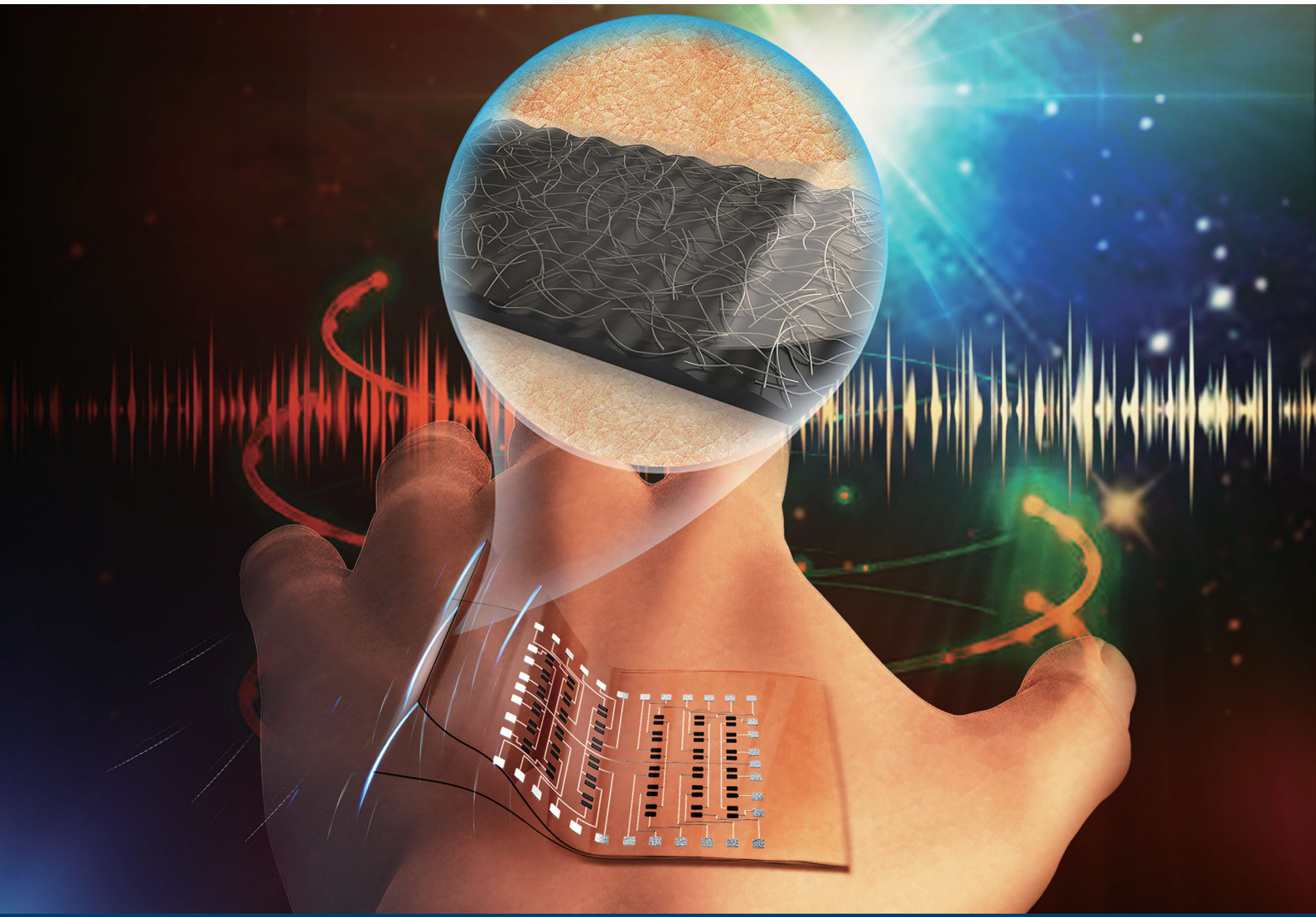

Themed issue: Celebrating Tobin Marks' 75th Birthday

ISSN 2050-7526

ROYAL SOCIETY OF CHEMISTRY

PAPER

Xinge Yu *et al.*
Stretchable transparent conductive elastomers for skin-integrated electronics

Journal of Materials Chemistry C

ROYAL SOCIETY OF CHEMISTRY

PAPER

View Article Online
View Journal | View Issue

Cite this: J. Mater. Chem. C, 2020, 8, 15105

Stretchable transparent conductive elastomers for skin-integrated electronics†

Zhan Gao, [a] Chunki Yiu,[a] Yiming Liu,[a] Dengfeng Li,[a] Liang Mei,[b] Zhiyuan Zeng [b] and Xinge Yu *[a]

Received 19th June 2020,
Accepted 22nd July 2020

DOI: 10.1039/d0tc02913k

rsc.li/materials-c

Electrodes with good mechanical and electrical properties serve as the key component for realizing high-performance flexible electronics. Here, we introduce a low-cost and scalable method with precise pattern control for producing intrinsically stretchable and transparent conductive elastomers based on silver nanowires (Ag NWs). The optimized electrodes in this work exhibit great transparence over 78%, a low sheet resistance of ~18 Ω sq^{-1} and remarkable mechanical properties without significant conductivity loss upon thousands of cycles of stretching, twisting, bending and pressing. The transparent Ag NWs can be precisely patterned onto a soft substrate at a microscale level and form a stretchable circuit. A skin-integrated electronic device with a 6 × 6 tactile sensor array was developed based on the resulting transparent and stretchable flexible circuit, indicating the possibility of the low lost and large area fabrication of electronic skin.

Introduction

Soft and transparent electrodes have been used for various flexible electronic devices, such as wearable electronics, deformable touch planes, flexible integrated circuits, electronic skin and bio-medical sensors.[1–6] Transparent electrodes for flexible electronics should fulfill the requirements of high optical transparency, high conductivity and stable mechanical performance under continuous and repeated deformations. Tin-doped indium oxide (ITO) has been widely used as a transparent electrode in both academia and industry; however, ITO does not meet the demands of flexible devices due to its intrinsic stiffness (fracturing after 1% strain) and the high cost of physical vapor deposition.[7–9] Therefore, novel alternative materials such as metal nanowires, graphene, conductive polymers, single-walled carbon nanotubes (CNTs) *etc.* have attracted much interest in recent years.[2,10–15] Exploring those materials into nano-structures, such as nano-fibers, nano-waves and nano-meshes, that enables improved conductivity and flexibility.[5,12–14] However, complicated micro-fabrication processes are typically used to form those nano-structures, which are not suitable for scalable, low-cost and large-area flexible electronics.[2] As one of the most promising conductive materials, silver nanowires (Ag NWs) exhibit high optical transparency, high electrical conductivity and great mechanical flexibility and thus have been proven to be excellent candidates for transparent and flexible electrodes.[16–20] Furthermore, Ag NWs can be deposited on a flexible substrate *via* various kinds of solution-based methods such as dip-coating, spin-coating and spray-coating, which have great potential in low-cost and scalable fabrication.[15,17–20]

The combination of Ag NWs with elastomers such as poly(dimethylsiloxane) (PDMS) to realize stretchable electrodes has received immense attention.[20–24] However, it is still a challenge to achieve high conductivity and mechanical stability simultaneously due to the poor adhesion between PDMS and Ag NWs. The hydrophobic nature of the PDMS surface can either cause aggregation of Ag NWs in direct film deposition processes, or a low coverage ratio in transfer printing processes,[22,25] which are two typical problems causing Ag NW delamination from PDMS after multiple cycles of mechanical deformations. Recent research using organic functional layers, such as poly(vinylalcohol)/glycerol, achieved a uniform dispersion of Ag NWs on PDMS, and realized transparent electrodes with good flexibility.[15] Moreover, Joo *et al.* developed a flexible electrode using a pre-stretched method to form multiscale-structured Ag NWs for capacitive type pressure sensing.[26] Similarly, a recent work on micro-wavy Ag NWs/PDMS with good mechanical properties obtained using a pre-stretched method was also reported for flexible capacitive type pressure sensors.[27] These results indicate that introducing a thin functional layer or pre-stretching is an effective route to improve the interfacial properties between Ag NWs and PDMS. However, considering the use of Ag NWs for functional flexible electronics, several challenges, such as low conductivity,

[a] Department of Biomedical Engineering, City University of Hong Kong, Hong Kong 999077, P. R. China. E-mail: xingeyu@cityu.edu.hk
[b] Department of Materials Science and Engineering, City University of Hong Kong, Hong Kong 999077, P. R. China

† Electronic supplementary information (ESI) available. See DOI: 10.1039/d0tc02913k

mechanical deformability, long-term stability, optical transparency, large surface areas and high cost, exist.

Here, we present material design and scalable pattern controlling strategies as a low-cost and efficient approach for obtaining an intrinsically stretchable transparent electrode. The transparent electrode is a conductive elastomer formed *via* spray-coating Ag NWs on a hexane treated pre-stretched PDMS substrate. The optimized transparent electrode exhibits great electrical, optical and mechanical properties, with transparency >78%, sheet-resistance as low as 18 Ω sq^{-1}, and robust flexibility without conductivity loss during hundreds to thousands of cycles of bending, pressing and stretching. The simple processing route enables a fast printing of flexible circuits that can be used for skin-integrated electronics. Demonstration of the stretchable electrode involved integration with a 6 × 6 tactile sensor array for electronic skin. These results suggest the broad potential application areas of this simple method in large-scale and low-cost wearable multifunction equipment and transparent flexible electronics.

Experimental

Fabrication of the soft transparent electrode

The glass substrate (2.5 × 7.5 cm^2) was cleaned in an ultrasonic bath with detergent water, acetone, deionized water, and isopropyl alcohol for 15 min each sequentially. PDMS (Sylgard 184, Dow Corning Corporation, crosslink : PDMS = 1 : 20) was drop-casted on the cleaned glass substrate and cured in an oven at 80 °C for 30 min to form a soft substrate (thickness ~ 0.5 mm). The soft substrate was first treated with energetic oxygen plasma (45 W) in a Harrick plasma cleaner for 3 min to create a hydrophilic surface, and then treated by spray-coating 2 mL of hexane solvent at a set air pressure of 10 psi to change the wettability. After the surface treatment, the PDMS substrate was laterally stretched to 150% by a stretcher. A Ag NW solution (Aladdin, average length: 40 μm, 5 mg mL^{-1} dispersed in ethanol) was spray-coated onto the pre-stretched substrate with a discharge speed of 40 μL/30 s by a USTAR S-120 spray gun (0.2 mm) connected with a METU Portable air pump at an air pressure of 30 psi and a distance of 10 cm, where the solution was stirred at 700 rpm for 1 h previously. After deposition of the Ag NWs, the PDMS substrate was released to its original state and annealed at 100 °C for 5 min to enhance the bonding strength between Ag NWs and PDMS. Finally, another layer of PDMS with the same thickness as the substrate as the top encapsulation layer was formed on the Ag NWs.

Fabrication of the tactile sensor array

The glass substrate (7 × 7 cm^2) was cleaned in an ultrasonic bath with detergent water, acetone, deionized water, and isopropyl alcohol for 15 min each sequentially. The fabrication started with the pre-treated PDMS substrate using the same processing procedure as that of the soft transparent electrode, but the PDMS substrate was tightly covered by a metallic mask film to form the designed flexible circuit pattern. The tactile sensor adopted a ternary elastomer composite format consisting of graphene (average powder thickness of 1.75 nm), CNTs (diameter, 10–20 nm; length, 10–30 μm) and Ecoflex. The composites were prepared by mixing 0.3 g of CNTs, 0.05 g of graphene and 17 g of Ecoflex together and stirring in a FlackTek DAC 330–100 speed mixer at 500 rpm for 2 h. Then, the ternary composite was blade-coated on the PDMS substrate *via* a metallic mask, followed by annealing at 150 °C in an oven for 30 min to form a 6 × 6 sensor array (an area of 2.5 × 3 mm^2 for each sensor). Finally, a PDMS encapsulation layer was drop-casted onto the soft substrate, followed by baking at 80 °C for 30 min.

Characterization and measurement

The surface morphologies of the Ag NW electrodes were measured using top-view scanning electron microscopy (SEM, FEI Quanta 450 FESEM) and a 3D Surface Profiler (Wyko NT9300) without the top encapsulation PDMS layer. The transmittance of the Ag NW electrode was characterized using a PerkinElmer Lambda 35 UV-VIS Spectrometer (air served as the background). The sheet resistance of the electrode was tested using a resistance tester (Helpass HPS2535). The resistance of the electrode under deformation was measured using a multimeter (Fluke F12E). The resistance variation of the tactile sensor array was measured using a Keysight B1500A Semiconductor Analyzer.

Results and discussion

Fig. 1a shows a schematic illustration of the fabrication process of the transparent and flexible electrode. Sufficient interconnected networks and strong adhesion between Ag NWs and the substrate are two key points for the high-performance Ag NW electrodes. The hydrophobic nature of the PDMS surface tends to engender the agglomeration and nonuniform dispersion of Ag NWs, resulting in poor electrical conductivity or even a locally open circuit.[25] Due to the weak bonding behavior between Ag NWs and PDMS, the conductivity of the electrode would significantly degrade during mechanical deformations. In this work, a two-step treatment method was introduced to overcome these shortcomings. The first step involved oxygen plasma treatment for introducing chemical functional groups (carbonyl, carboxyl, and hydroxyl) to enhance the hydrophilic property of PDMS.[28] However, the PDMS surface is thermodynamically unstable since the low molecular weight chains (uncross-linked PDMS chains or residual crosslinking agent) may diffuse to the surface of PDMS, which could change surface property from hydrophilic to hydrophobic again.[29–31] Thus, the second treatment step involved the pre-spraying of hexane solvent to extract and remove these low molecular weight chains, and this ensured the hydrophilic property of the PDMS surface.[32–34] Fig. 1b and Fig. S1 (ESI†) show SEM images of the Ag NW networks deposited on PDMS, where it can be found that the Ag NW networks orientate perpendicular to the pre-stretching direction. This phenomenon can be explained as the Ag NW networks spontaneously buckled during the relaxation of the pre-stretched PDMS, and the corresponding evidence can be

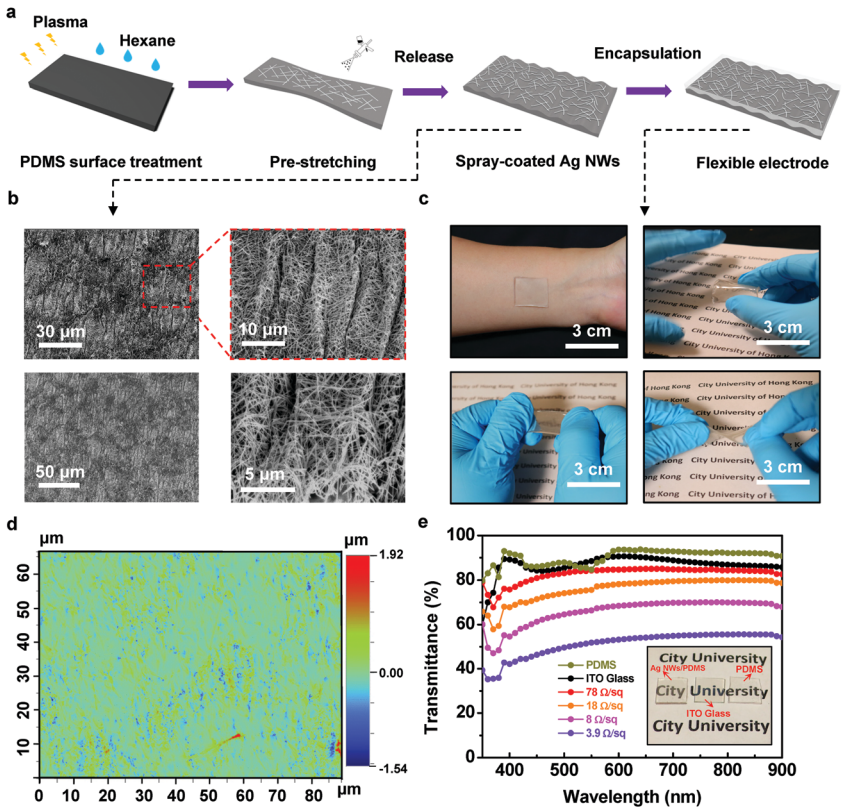

Fig. 1 Thin, soft and transparent conductive elastomers. (a) Schematic illustration of the fabrication process. (b) Top-viewed SEM images of the Ag NW networks on the buckled PDMS surface at different scales. (c) Optical images of the flexible electrode under various deformations. (d) Surface profile characterizations of the Ag NW film. (e) Optical transmittance spectra of the flexible electrode. The inset shows an optical image of Ag/NWs, ITO glass and pure PDMS for comparison.

found in the enlarged SEM images in Fig. 1b. The slightly buckled Ag NWs demonstrate strong bonding behavior between Ag NWs and PDMS that makes the transparent electrode more flexible and stretchable. Enlarged views of the morphology show that some island-like structures in the Ag NW networks are formed after releasing the pre-strain (Fig. S2, ESI†), which can enhance the conductivity over a large area. The surface profile characterizing the surface roughness of the Ag NW networks (Fig. 1d) provides an average root mean square (RMS) roughness of 121 nm, which was due to the buckled structures of the Ag NW networks. A further decrease of the roughness would require balancing the conductivity and transparency of the Ag NWs. The transparent electrode in this work exhibits superior flexibility that can be conformably integrated with human skin (Fig. 1c).

The conductivity and optical transparency are two key parameters for transparent flexible electrodes, which are both dominated by the duration of coating. Fig. 1e summarizes the sheet resistance and optical transparency of the Ag NWs. It is well known that the gaps among Ag NW networks allow light to pass through. Therefore, the density of Ag NWs is highly relevant to the optical transparency, where thicker networks exhibit lower sheet resistance but poorer transparency and *vice versa*. So, a balance between these two indexes is critical. With a very slow discharge speed of 40 μL/30 s, we can easily control the thickness of the Ag NW film, thus controlling both conductivity and optical transparency by varying the duration of coating. A longer coating duration could result in a thicker

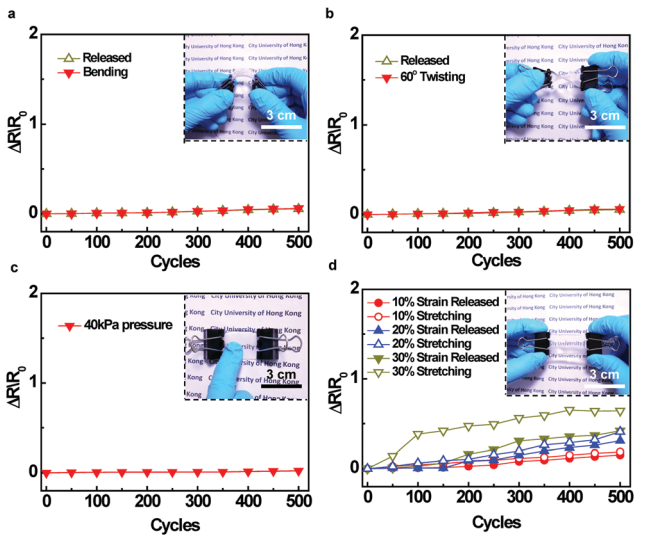

Fig. 2 Mechanical property measurement of the flexible electrode. Resistance variation of the electrode under different mechanical deformations: (a) bending tests; (b) twisting tests; (c) pressing tests and (d) stretching tests. Inset images show the device under various kinds of testing conditions.

Table 1 Performance summary of the recently reported Ag NW based conductors

Materials	Conductivity (Ω sq^{-1})	Bending tests[a]	Twisting tests[a]	Stretching tests[a]	Transparency (%)	Ref.
Ag NW: PEDOT:PSS	5.4	—	—	—	94	17
Ag NW	4.5	—	—	20%, 50	80	22
Ag NW mesh	6.5	—	—	—	91	35
Ag NW: cellulose	56	150°, 3000	—	—	90	36
Ag NW	16	—	60°, 1000	20%, 800	87	37
Ag NW	15.6	—	—	—	84	38
Ag NW	14	300	300	25%, 300	50.57	39
Ag NW	18	90°, 2500	60°, 2000	20%, 1800	78	This work

[a] Deformation level applied during the cyclic test (left) if any and the number of cycles (right) after significant conductive loss.

Ag NW film and greater conductivity but poorer transparency. Table S1 (ESI†) summarizes the conductivity and optical transparency of the electrodes corresponding to different coating durations. Here, the optimized electrode was achieved by adjusting the spray-coating duration to about 20 s to realize transparency greater than 78% over the visible spectrum and a low sheet resistance of 18 Ω sq^{-1}, which is compatible to that of ITO coated glass (inset of Fig. 1e).

The mechanical properties of our transparent flexible electrode were studied by analyzing the resistance variation $\Delta R/R_0$ ($\Delta R = R - R_0$, where R is the tested resistance under various deformations and R_0 is the initial resistance before deformation). Fig. 2 and Fig. S3 (ESI†) summarize the resistance variation of the electrode under bending, twisting, pressing and stretching conditions. For the bending test, the electrode shows very stable conductivity with the resistance remaining even after 1000 cycles of bending ($\Delta R/R_0 = 0.09$ at the 1000th cycle). These excellent mechanical properties under bending conditions could be attributed to the buckled structure of the Ag NW networks, which can significantly suppress the slipping or delamination of the Ag NW junctions and maintain their conductivity. Similarly, the electrode also exhibits great tolerance to twisting, with a negligible variation value of 0.067 after 500 cycles and a slight variation value of 0.21 after 1000 cycles. In the pressing test, we pressed the middle of the electrode using a finger with an estimated pressure of 40 kPa. As shown in Fig. 2c, the resistance of the electrode remains unchanged and the resistance variation is only 0.011 after 500

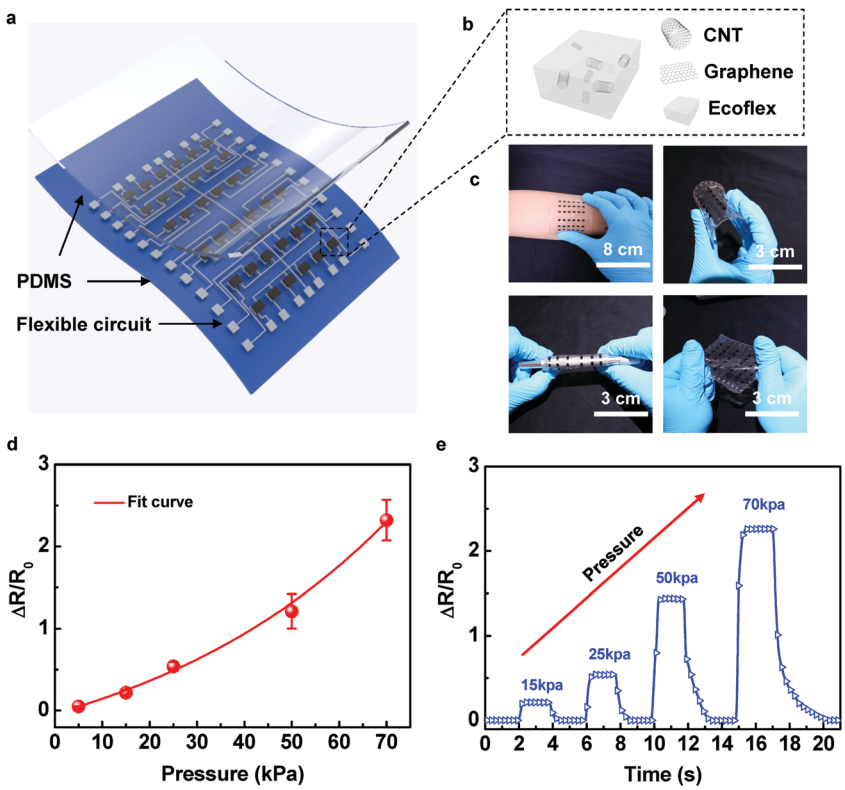

Fig. 3 Flexible circuit based on Ag NWs for a 6 × 6 tactile sensor array. (a) Schematic illustration of the device structure. (b) Schematic illustration of the ternary piezoresistive component, consisting of graphene, CNTs and Ecoflex. (c) Optical images of a sensor array attached on skin and under different deformations. (d) Resistance variation as a function of pressure of the single pressure sensor. (e) Dynamic pressure response measurements of single piezoresistive sensors with increasing pressure.

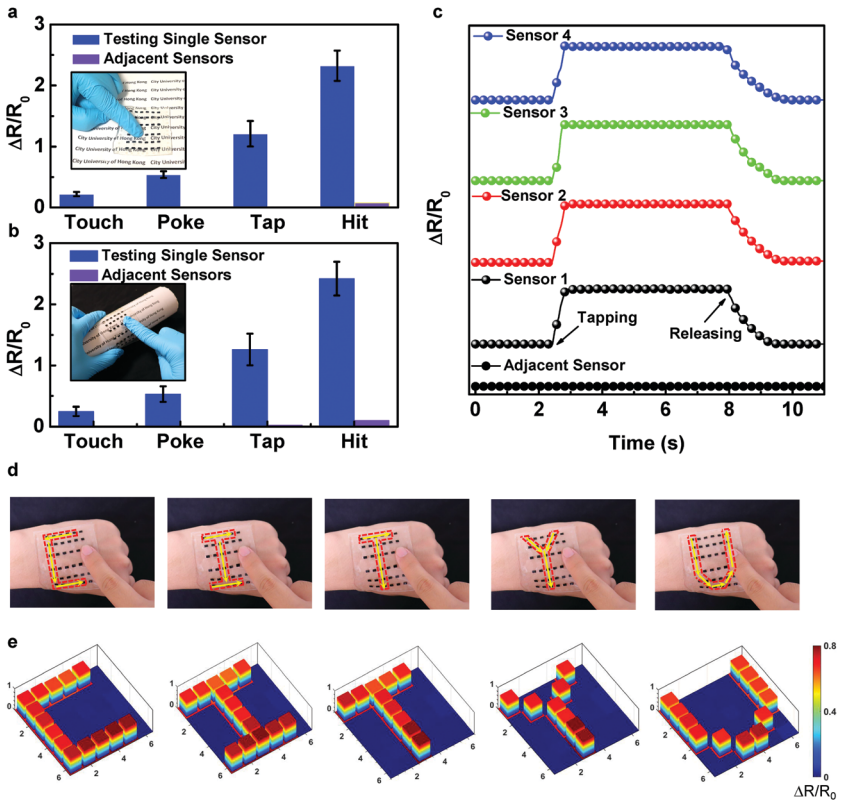

Fig. 4 Tactile mapping of the 6 × 6 tactile sensor array. Resistance variation measurement of a single piezoresistive component and its adjacent sensors on (a) flat and (b) curved surfaces, with inset showing optical images of the test conditions. (c) Dynamic pressure response measurements of 4 different sensors and their adjacent sensors. (d) Optical images of the sensor array mounted on the surface of a human hand, showing the positions and sequence of external pressure. (e) Corresponding resistance variation distributions with a "CITYU" pattern.

cycles of pressing. Such a negligible resistance variation under pressing is crucial in the application of piezoresistance pressure sensors, which can eliminate the undesired influence and coupling induced by the resistance variation of the electrodes. Note, the measurement of resistance was performed both under the mechanical deformation and after releasing, and the results show that the resistance of the Ag NW electrode is unchanged during and after the processes of bending, twisting and pressing. Fig. 2d shows the results of the stretching test under 10%, 20% and 30% strain. A good durability under 10% strain and 20% strain for multiple cycles of stretching can be observed, with a slight increase of resistance after 500 cycles of stretching. Furthermore, the resistance of the electrode is almost the same during stretching and after releasing. When the strain increases to 30%, the electrode could still maintain the same conductivity after 100 cycles of stretching but it showed a gradual increase in sheet resistance for more cycles of stretching. The variation in resistance at a higher strain level shows a large difference during stretching and after releasing with variations of 0.64 and 0.41 at 500 cycles of stretching and after releasing, respectively. The deterioration of conductivity could be attributed to the delamination of the Ag NW networks at a higher strain level and therefore this causes a reduction of the number of effective Ag NWs per unit area. However, a further increase in the stretching to 50% causes a significant performance deterioration after multiple cycles of testing (Fig. S3d, ESI†), which is because of the fact that the testing strain level is equal to the pre-strain level of the substrate during the preparation of the Ag NWs. Since the transparent electrode in this work aims for e-skin applications, 20–30% stretching is the targeted maximum strain level due to the nature of skin mechanics. Future works on further improving the stretchability at greater stain levels could consider increasing the pre-strain level of the substrate during Ag NW deposition. The Ag NW network based electrode in this work shows remarkable robustness under bending, twisting, pressing and low strain level stretching compared to the reported Ag NW based transparent electrodes (Table 1),[17,22,35–39] which provides the possibility for serving as flexible circuits of skin-integrated electronics.

Taking advantage of the remarkable mechanical properties of the flexible Ag NW electrode, we designed a flexible circuit based on a simple processing route. This circuit was realized by directly spray-coating Ag NWs though a mask (details are in the Experimental section), which served as electrodes and interconnects with a conductive path as narrow as 200 μm (Fig. 3a). Here, a 6 × 6 tactile sensor array based on piezoresistive composites was used to demonstrate the application of the Ag NW elastomer (Fig. 3a). The tactile sensors adopted a widely reported strategy, wherein intrinsically stretchable Ecoflex served as the elastomer precursor for blending with graphene

and carbon nanotubes (Fig. 3b).[40–46] In this work, the sensing area was defined as 2.5×3 mm^2 for each tactile sensor, and the overall working area of the tactile sensor array is 3×3 cm^2. As illustrated in Fig. 3c, the tactile sensor array exhibits great flexibility and can be bended, wrapped on a tube, stretched or even attached onto the skin as electronic-skin. The single tactile sensor was first characterized and calibrated at various pressures, as shown in Fig. 3d, where the resistance variation of the sensor shows a clear relationship with the loaded pressure. Fig. 3e shows the dynamic time dependent plots of resistance variations under different pressure values, where we find the response time of the sensor to be $\sim$0.25 s under all levels of pressure and that the resistance could recover to its initial value after the removal of the applied pressure. Next, the resistance variations of one representative sensor in the array and its adjacent sensors were measured using four different tactile methods, touching ($\sim$15 kPa), poking ($\sim$25 kPa), tapping ($\sim$50 kPa) and hitting ($\sim$70 kPa) (Fig. 4a and b). The measurement was performed on a flat platform and we can clearly distinguish the difference for the different tactile forces. Furthermore, the adjacent sensors did not show any resistance variations under gentle touching conditions, while hard and forceful touching, *i.e.* hitting, only induced a slight coupling response (average $\Delta R/R_0 = 0.08$), indicating almost no cross-talk among the adjacent sensors.

Benefiting from the great mechanical properties of the flexible Ag NW electrode, the sensor array can also be used on curved surfaces and under stretched conditions, and shows the same response behaviors with almost the same resistance changes as that measured on flat surfaces (Fig. 4b and Fig. S4, ESI†). Fig. 4c shows the $\Delta R/R_0$ – time plots for 4 sensors (simultaneously applied with pressure, as shown in Fig. S5b, ESI†) and adjacent sensors without pressure. The 4 measured sensors exhibit similar resistance variations and response times to pressure while the adjacent sensors do not couple with the tested sensors. Fig. 4e presents the e-skin functions of this sensor array, where a finger pressed "CITYU" pattern is observed on the device. As a finger pressed the selected sensors by roughly equal pressure sequentially, the sensor array demonstrated clear tactile mapping with a resistance variation of 0.6–0.8. Such results indicated that more vivid tactile mapping could be realized by increasing the sensor channel counts.

Conclusion

In summary, we developed a simple, low-cost and scalable approach with precise pattern control for producing intrinsically soft transparent electrodes based on Ag NWs. Detailed measurements and theoretical investigations have highlighted the remarkable optical, electrical and mechanical properties of the soft transparent electrodes. Furthermore, flexible circuits with finely designed patterns were produced, which formed large-area flexible pressure sensor arrays. The results presented here align with low cost flexible electronics, offer potential possibilities in high throughput and large area e-skin production, flexible displays and many others.

Conflicts of interest

There are no conflicts of interest to declare.

Acknowledgements

This work was supported by the City University of Hong Kong (Grants No. 9610423 and 9667199), Research Grants Council of the Hong Kong Special Administrative Region (Grant No. 21210820), and Science and Technology Bureau of Sichuan Province (Grant No. 2020YFH0181).

References

1 X. Yu, Z. Xie, Y. Yu, J. Lee, A. Vazquez-Guardado, H. Luan, J. Ruban, X. Ning, A. Akhtar, D. Li, B. Ji, Y. Liu, R. Sun, J. Cao, Q. Huo, Y. Zhong, C. Lee, S. Kim, P. Gutruf, C. Zhang, Y. Xue, Q. Guo, A. Chempakasseril, P. Tian, W. Lu, J. Jeong, Y. Yu, J. Cornman, C. Tan, B. Kim, K. Lee, X. Feng, Y. Huang and J. A. Rogers, *Nature*, 2019, **575**, 473–479.
2 T. Sekitani, H. Nakajima, H. Maeda, T. Fukushima, T. Aida, K. Hata and T. Someya, *Nat. Mater.*, 2009, **8**, 494–499.
3 X. Yu, H. Wang, X. Ning, R. Sun, H. Albadawi, M. Salomao, A. C. Silva, Y. Yu, L. Tian, A. Koh, C. M. Lee, A. Chempakasseril, P. Tian, M. Pharr, J. Yuan, Y. Huang, R. Oklu and J. A. Rogers, *Nat. Biomed. Eng.*, 2018, **2**, 165–172.
4 S. Wang, J. Xu, W. Wang, G. N. Wang, R. Rastak, F. Molina-Lopez, J. W. Chung, S. Niu, V. R. Feig, J. Lopez, T. Lei, S. Kwon, Y. Kim, A. M. Foudeh, A. Ehrlich, A. Gasperini, Y. Yun, B. Murmann, J. B. H. Tok and Z. Bao, *Nature*, 2018, **555**, 83–88.
5 B. Wang, A. Thukral, Z. Xie, L. Liu, X. Zhang, W. Huang, X. Yu, C. Yu, T. J. Marks and A. Facchetti, *Nat. Commun.*, 2020, **11**, 2405.
6 K. Zhang, Y. H. Jung, S. Mikael, J. Seo, M. Kim, H. Mi, H. Zhou, Z. Xia, W. Zhou, S. Gong and Z. Ma, *Nat. Commun.*, 2017, **8**, 1782.
7 K. A. Sierros, N. J. Morris, K. Ramji and D. R. Cairns, *Thin Solid Films*, 2009, **517**, 2590–2595.
8 Z. Chen, B. Cotterell and W. Wang, *Eng. Fract. Mech.*, 2002, **69**, 597–603.
9 X. Yu, T. J. Marks and A. Facchetti, *Nat. Mater.*, 2016, **15**, 383–396.
10 W. He, Y. Sun, J. Xi, A. A. M. Abdurhman, J. Ren and H. Duan, *Anal. Chim. Acta*, 2016, **903**, 61–68.
11 A. Rabti, C. C. Mayorga-Martinez, L. Baptista-Pires, N. Raouafi and A. Merkoçi, *Anal. Chim. Acta*, 2016, **926**, 28–35.
12 Z. Chen, W. Ren, L. Gao, B. Liu, S. Pei and H. Cheng, *Nat. Mater.*, 2011, **10**, 424–428.
13 S. D. Perera, B. Patel, N. Nijem, K. Roodenko, O. Seitz, J. P. Ferraris, Y. J. Chabal and K. J. Balkus, *Adv. Energy Mater.*, 2011, **1**, 936–945.
14 K. Gopalsamy, Z. Xu, B. Zheng, T. Huang, L. Kou, X. Zhao and C. Gao, *Nanoscale*, 2014, **6**, 8595–8600.
15 J. Sun, W. Zhou, H. Yang, X. Zhen, L. Ma, D. Williams, X. Sun and M. Lang, *Chem. Commun.*, 2018, **54**, 4923–4926.
16 S. Yun, X. Niu, Z. Yu, W. Hu, P. Brochu and Q. Pei, *Adv. Mater.*, 2012, **24**, 1321–1327.

17 J. Kim, D. Ouyang, H. Lu, F. Ye, Y. Guo, N. Zhao and W. C. H. Choy, *Adv. Energy Mater.*, 2020, **10**, 1903919.
18 T. Akter and W. S. Kim, *ACS Appl. Mater. Interfaces*, 2012, **4**, 1855–1859.
19 V. Scardaci, R. Coull, P. E. Lyons, D. Rickard and J. N. Coleman, *Small*, 2011, **7**, 2621–2628.
20 H. Kim, M. Patel, H. Park, A. Ray, C. Jeong and J. Kim, *ACS Appl. Mater. Interfaces*, 2016, **8**, 8662–8669.
21 S. Kang, T. Kim, S. Cho, Y. Lee, A. Choe, B. Walker, S. Ko, J. Y. Kim and H. Ko, *Nano Lett.*, 2015, **15**, 7933–7942.
22 J. Wang, C. Yan, W. Kang and P. S. Lee, *Nanoscale*, 2014, **6**, 10734–10739.
23 T. Akter and W. S. Kim, *ACS Appl. Mater. Interfaces*, 2012, **4**, 1855–1859.
24 C. Lim, Y. Shin, J. Jung, J. H. Kim, S. Lee and D. Kim, *APL Mater.*, 2019, **7**, 31502.
25 D. Choi, H. Kang, H. Sung and S. Kim, *Nanoscale*, 2013, **5**, 977–983.
26 Y. Joo, J. Byun, N. Seong, J. Ha, H. Kim, S. Kim, T. Kim, H. Im, D. Kim and Y. Hong, *Nanoscale*, 2015, **7**, 6208.
27 L. Ma, X. Shuai, Y. Hu, X. Liang, P. Zhu, R. Sun and C. Wong, *J. Mater. Chem. C*, 2018, **6**, 13232.
28 A. W. Adamson, *Physical Chemistry of Surfaces*, John Wiley, New York, 1990, vol. 20, 525–535.
29 J. A. Vickers, M. M. Caulum and C. S. Henry, *Anal. Chem.*, 2006, **78**, 7446–7452.
30 B. Cortese, S. D'Amone, M. Manca, I. Viola, R. Cingolani and G. Gigli, *Langmuir*, 2008, **24**, 2712–2718.
31 D. T. Eddington, J. P. Puccinelli and D. J. Beebe, *Sens. Actuators, B*, 2006, **114**, 170–172.
32 Y. Meng, Z. B. Li, X. Chen and J. P. Chen, *Microelectron. Eng.*, 2014, **130**, 8–12.
33 S. Kumagai and N. Yoshimura, *IEEE Trans. Power Delivery*, 2003, **18**, 506–516.
34 J. W. Chang and R. S. Gorur, *IEEE Trans. Dielectr. Electr. Insul.*, 1994, **1**, 1039–1046.
35 J. Groep, P. Spinelli and A. Polman, *Nano Lett.*, 2012, **12**, 3138–3144.
36 R. Li, K. Zhang and G. Chen, *Materials*, 2019, **12**, 322.
37 W. Chen, F. Li and G. Liou, *Adv. Opt. Mater.*, 2019, **7**, 1900632.
38 S. Biswas, H. Sano, X. Yang, S. Tanpichai, M. Shams and H. Yano, *Adv. Opt. Mater.*, 2019, **7**, 1900532.
39 X. Ding, H. Cao, S. Sun, M. Li and H. Liu, *High Perform. Polym.*, 2019, **31**, 1153–1161.
40 S. A. Chowdhury, M. C. Saha, S. Patterson, T. Robison and Y. Liu, *Adv. Mater. Technol.*, 2019, **4**, 1800398.
41 K. Ke, M. McMaster, W. Christopherson, K. D. Singer and I. Manas-Zloczower, *Composites, Part A*, 2019, **126**, 105614.
42 C. Liu and J. Choi, *J. Micromech. Microeng.*, 2009, **19**, 85019.
43 D. J. Lipomi, M. Vosgueritchian, B. C. Tee, S. L. Hellstrom, J. A. Lee, C. H. Fox and Z. Bao, *Nat. Nanotechnol.*, 2011, **6**, 788–792.
44 H. Kou, L. Zhang, Q. Tan, G. Liu, H. Dong, W. Zhang and J. Xiong, *Sci. Rep.*, 2019, **9**, 3916.
45 Y. Liu, L. Zhao, L. Wang, H. Zheng, D. Li, R. Avila, K. W. C. Lai, Z. Wang, Z. Xie, Y. Zi and X. Yu, *Adv. Mater. Technol.*, 2019, **4**, 1900744.
46 S. Woo, J. Kong, D. Kim and J. Kim, *J. Mater. Chem. C*, 2014, **2**, 4415–4422.